1988

NASA/ASEE SUMMER FACULTY FELLOWSHIP PROGRAM

MARSHALL SPACE FLIGHT CENTER
THE UNIVERSITY OF ALABAMA

Angular Response Calibration of the Burst And Transient Source Experiment

Prepared by:	John Patrick Lestrade
Academic Rank:	Assistant Professor
University and Department:	Mississippi State University Department of Physics and Astronomy

NASA/MSFC:

Laboratory:	Space Science
Division:	Astrophysics
Branch:	High-Energy Astrophysics
MSFC Colleague:	G. J. Fishman
Date:	July 29, 1988
Contract No.:	NGT 01-002-099 University of Alabama

Angular Response Calibration of the Burst And Transient Source Experiment

by

John Patrick Lestrade
Assistant Professor of Physics and Astronomy
Mississippi State University
Mississippi State, Mississippi, 39762

Abstract

The Gamma Ray Observatory includes four experiments designed to observe the gamma-ray universe. Jerry Fishman in the High Energy Astrophysics Branch at Marshall Space Flight Center is the principal investigator for one of these experiments, the Burst And Transient Source Experiment (BATSE).

We have recently completed laboratory measurements to test the response of the BATSE modules to gamma-ray sources that are non-axial. The results of these observations are necessary for the correct interpretation of BATSE data obtained after it is put in Earth orbit. The launch is planned for March, 1990.

Preliminary analyses of these test data show the presence of a radial dependence† to the detector's light collection efficiency. As a continuation of the work begun as a NASA/ASEE Summer Faculty Fellow, we propose to evaluate the importance of this radial response, analyze future experimental data to derive the actual functional dependence on radius, and calculate the net effect on the output spectrum as a function of the angle of incidence.

† The dependence is radial in the sense that energy-depositing events that cause scintillation near the center of the 20-inch diameter disc are more efficiently collected than those events near the edge.

Acknowledgement:

This past summer has been an invaluable experience for me, both professionally and personally. The BATSE team have given unselfishly of their time and expertise to make me an integral part of the group. I appreciate all that I have learned from them. I am sincerely grateful for their acceptance and friendship.

In particular I would like to thank Jerry Fishman. His knowledge and enthusiasm have been very helpful. His guidance throughout this summer is responsible for the positive results that I have obtained.

This experience would not have been realized if it were not for the friendship and help of Ernestine Cothran and Michael Freeman. As coordinators of the program, they are responsible for my participation.

Pat Lestrade
July 29, 1988

List of Figures

1. Introduction:

1.1 The Gamma-Ray Observatory

Before the year 2000 NASA plans to launch more than 9 major space missions. These observatories will study the universe in the infrared, visible, ultraviolet, x-ray, and gamma-ray portions of the spectrum. The objects to be studied include the earth, the planets, the sun, and other more exotic, cosmological objects in which high-energy processes are taking place. Some of the objects will be well known, at least theoretically, such as pulsars. Others, for example, gamma-ray bursters, are mysterious and enigmatic.

One of these future satellites is the Gamma-Ray Observatory (GRO). Shown in Figure 1, GRO is a 17-ton satellite carrying 4 experiments; the Oriented Scintillation Spectrometer Experiment (OSSE), the Imaging Compton Telescope (COMPTEL), the Energetic Gamma-Ray Experiment (EGRET), and the Burst And Transient Source Experiment (BATSE). Together, these instruments detect gamma radiation at energies from 30 keV to 30 GeV. GRO is scheduled to be launched in March of 1990 to a nominal altitude of 250 miles (400 km). Its expected lifetime is from two to ten years.

The High-Energy Astrophysics Branch in the Space Science Laboratory at Marshall Space Flight Center has designed, built, and is now testing the BATSE detectors. As a NASA/ASEE Summer Faculty Fellow I have been involved in some of the laboratory testing of the BATSE modules and in the preliminary analysis of the acquired data.

1.2 Burst And Transient Source Experiment

BATSE is composed of eight detector modules (cf. Figure 2). These modules will be situated at the eight 'corners' of GRO. In this orientation it is able to monitor the complete sky except for that part temporarily blocked by the earth. As the name implies, BATSE is designed to observe and record gamma-ray events that are short-lived. The principal transient source to be studied will be gamma-ray bursters. At the same time, it has the ability to observe sources of gamma radiation that are long-lived – such as the sun, pulsars, and black holes.

The principal detector in each module, called the Large-Area detector (LAD), is a sodium iodide crystal in the shape of a disc with a diameter of 20 inches and a thickness of 0.5 inches. The shape and size of the crystal were chosen to make

BATSE more sensitive to the low-energy gamma ray spectrum (i.e., 30 keV$\sim$ 1.8 MeV) and to permit the measurement of very weak sources.

Also shown in Figure 2, in front of the LAD, is a charged-particle detector (CPD) consisting of a plastic scintillator. Charged particles such as cosmic rays that deposit energy in the LAD will also be recorded in the CPD. Electronic coincidence circuitry is used to exclude these events from the recorded spectra.

In addition to the main crystal, there is a secondary detector called the Spectroscopy detector (SPD). It too is composed of sodium iodide, 3-inches thick with a 5-inch diameter. Because of its greater thickness, it extends the sensitivity to higher energies ($\approx$ 25 MeV). It also has significantly better resolution than does the LAD.

1.2.1 BATSE Testing and Calibration

One of the problems inherent in an observational science is the effect that the observer's instrument has on the data. All instruments have what is called a 'point-spread function'. That is, given a uniquely-valued input, the output contains a finite spread in values reflecting the instrument's resolution. In the case of a gamma-ray instrument, such as BATSE, there are contributions to this dispersion from inhomogeneities in the crystal, from statistical fluctuations in the conversion of gamma-ray energy into an electrical signal, from electronic noise, and from other sources. Each contribution tends to spread the monoenergetic input into an approximate gaussian shape. An example of the resultant 'photopeak' is shown in Figure 3. However, the results are further complicated by scattering events which result in only partial deposition in the crystal. The total 'spread' is much more complicated.

When a monoenergetic beam of photons strikes the sodium iodide crystal in the detector, some of the photons are completely converted into an electrical response that becomes recorded as counts in one of the channels of the photopeak (see Figure 3). However, some photons deposit only part of their energy and are scattered out of the detector. These become recorded as lower-energy events and show up as counts in the Compton continuum. Still other photons lose some energy outside of (often behind) the crystal and are then scattered back into the crystal where they become recorded as counts in the backscatter peak. As seen in this figure, even when the input is monoenergetic, these effects distort the spectrum in a very complicated way. When the source is *not* monoenergetic the situation is considerably more complicated.

Figures 4 and 5 present observations of two typical gamma-ray bursters†. The first, from a Spacelab 2 measurement on Aug. 5, 1985, shows that the duration of

† Harding *et. al.*

a burst is on the order of seconds. The next figure (5) shows the spectrum of a burster on Mar. 7, 1979. The exponential spectrum is typical of these events and is consistent with a model based on thermal bremstrahlung. These are certainly more complicated than the monoenergetic case. Before we can determine the true spectrum that was *incident* on the detector, we must solve a complicated problem that depends on how the detector responds to incident photons. This response is a function of not only the incident energy but also of the angle of incidence. The task of developing this deconvolution software has been assigned to a BATSE co-investigator at the Goddard Space Flight Center. At MSFC part of our responsibility is to provide a response matrix that describes the detector's effects on an input spectrum. To this end we have spent the last few months measuring the spectra of several sources under various conditions. This report outlines some of those measurements and proposes some tests and procedures for the future.

2. Past Work

2.1 Angular Response: TPS-19

During a gamma-ray event for BATSE in earth orbit there are at least four detectors responding to the flux of radiation. Since these detectors are oriented in different directions, it is important to know how the response changes as a function of the angle of the incident flux.

The most important factor in this response is the projected area of the detector face to the radiation. This should, and does, impose a (co)sinusoidal response. However, there are several other significant factors that affect the response.

The first of these is an effect that counteracts the cosine decrease. At near-normal incidence ($\theta = 0°$) as the angle increases there is an *increase* in the deposition probability for photons entering the 0.5-inch thick crystal due to the increasing slant path. This opposes the decrease in absorption caused by the decrease in projected area. To a first approximation the angular response near 0° is

$$\cos\theta \cdot \left(1 - e^{-\tau/\mu}\right) \tag{1}$$

where $\mu = \cos\theta$. For sodium iodide the absorption coefficient at 662 keV, is approximately 0.71 in^{-1} (0.28 cm^{-1}). This gives a τ of 0.36 for a half-inch normal thickness. This function (1) and the cosine function are plotted in Figure 6. Measurements of spectra to be shown below will verify this slant-path effect.

The second factor arises because the detector has a finite thickness. Therefore, even at an angle of incidence of 90°, there is some deposition of energy in the crystal. Figure 7 presents observations of the height of the cesium-137 662 keV photopeak as a function of angle. At 90° the data are non-zero.

The third effect is seen at angles greater than 90°. It is due to the complicated scattering and absorption introduced by the material behind the crystal. At high enough energies (i.e., > 150 keV) some radiation is still deposited in the crystal. However, it is attenuated compared with that at 0°. A later figure covering 360° will show more structure because of the heterogeneous distribution of the electronics.

2.2. Experimental Considerations

Ideally, we would like to be able to irradiate the instrument with a monoenergetic beam of gamma rays with a constant flux. This would make the analyses

of the output spectra a simpler task. As mentioned above, however, even such a simple beam produces a complicated spectrum. In addition, this "response" will vary as the instrument is turned with respect to the incident beam. In order to get the perfect response matrix therefore, we would have to repeat those measurements for all angles and at all energies.

In practice we have to limit the number of laboratory measurements. For obvious reasons we can record spectra at only a finite number of angles and for a finite number of incident energies.

The table below lists the radioactive sources used in this test. There is the added complication that these sources do not, for the most part, emit a monoenergetic beam. This causes spectral features to "ride" on top of others complicating the analysis. The MSFC test identification number for these angular response tests is MSFC-BATSE-TPS-19.

Radioactive Sources Used for BATSE Testing

Isotope	${}^{A}_{Z}$Symbol	Half-Life	Energies (MeV)*
Americium-241	${}^{241}_{95}$Am	458 yr.	0.060
Barium-133	${}^{133}_{56}$Ba	7.2 yr.	0.032, <u>0.080</u>, 0.276, <u>0.302</u>, <u>0.356</u>
Cadmium-109	${}^{109}_{48}$Cd	453 d.	0.023, 0.088
Cesium-137	${}^{137}_{55}$Cs	30.0 yr.	0.032, 662
Cobalt-60	${}^{60}_{27}$Co	5.62 yr.	<u>1.173</u>, <u>1.332</u>, [2.505]
Cobalt-57	${}^{57}_{27}$Co	270 d.	<u>0.014</u> , <u>0.122</u>, 0.136
Selenium-75	${}^{75}_{34}$Se	-	0.121, 0.265, 0.401
Sodium-22	${}^{22}_{11}$Na	2.62 yr.	<u>0.511</u>, <u>1.275</u>, [1.786]
Thorium-232	${}^{232}_{90}$Th	1.4×10^{10} yr.	2.615, others

* underscore indicates coincident gammas, square brackets indicate sum peaks.

Figure 8 shows the angles chosen for measurement. The regions around 90° and 270° are of particular importance, so they received special attention. At each of these 40 angles a five-minute spectrum was recorded for each source. A background spectrum was then subtracted before storing them on $5\frac{1}{4}$-inch floppy disks (cf. Appendix A).

2.3. Data Analysis

Figures 9 and 10 show the effects of incidence angle on the spectrum of Cesium-137 as measured by both the Spectroscopy detector (SPD) and the Large-Area detector (LAD). Note the sharper resolution of the spectroscopy detector for the line at 662 keV. Also note the smaller backscatter peak for the very thick spectroscopy detector. Very few photons penetrate through the SPD to be scattered back into the crystal. Also evident in the photopeak of Figure 10 is the slant-path effect mentioned in §2.1. The curve for 45° is not $1/\sqrt{2}$ times that at 0° – as would be expected from a pure $\cos\theta$ decrease.

In order to simplify the study of the dependence on the angle of incidence, we concentrated on three parameters; 1) peak centroid, 2) peak resolution, and 3) peak height. It is obvious that the height and resolution should show a dependence on angle. We expect the peak to decrease in size due to the decreasing intercepted flux. Further, we would expect the resolution (R =FWHM/Energy) to become degraded (i.e., increase) as the angle gets closer to 90°. These effects are seen. However, it is not obvious that the peak centroid should show an angular dependence. In the first approximation, the peak centroid reflects the energy of the incident gamma ray. Since this energy is *independent* of the angle of incidence, the angle is not expected to have an effect on the position of the centroid. That would be true if the crystal were spatially homogeneous in its response to energy deposition. This apparently is not the case.

2.3.1 Radial Response

In actual fact, the detectors are known to possess what we have termed a "radial response" function. This function represents the fact that energy deposited near the perimeter of the detector has a light collection efficiency that is roughly 15% less than for that deposited near the center. This is not a property of the scintillator, but rather, a property of the light-collection process. Therefore, when the crystal is illuminated, the output is a superposition of gaussians, not centered about the true centroid, but shaded to the left (i.e., lower energies).

The most interesting effects of this radial response occur for angles of incidence near 90°. First, since the photons that are totally converted in the crystal are deposited near the edge, the system responds with a gaussian that is representative of that region near the perimeter. The output therefore indicates a lower energy than that of the incident photon. The result is a photopeak that is lower in energy so its centroid is shifted to the left of where it should be.

In addition to the lowering of the output peak centroid energy, the output does not contain the large variation in centroids which are present when the illumination

is normal (i.e., 0°). The result at $\theta = 90°$ and 270° is a photopeak with a truer gaussian shape.

Both of these effects are seen in Figures 11 and 12. These present the 662 keV peak at angles of 0° and 266°. Note that at 0° the peak is a superposition of many different gaussians representing the contributions from all parts of the crystal. The theoretical gaussian shown in Figure 11 has a centroid at 662 keV. The data at 266°, on the other hand, peak at a lower energy, are less dispersed, and show a purer gaussian shape because they arise from a more localized region of the crystal.

2.3.2 Results

Figure 13 presents the centroid of the photopeak as a function of angle of incidence. Note the sharp drop in position near 90° and 270° for the cesium peak. We have also plotted on this graph partial measurements for lower energy radiation. For the 88 keV and 265 keV lines it was difficult to measure the peak centroids at angles greater than 80° because of blending or lack of penetration through the back of the detector. Still the trends of these two are similar to that of the cesium line.

We have also measured the resolutions (FWHM/Energy) of the cesium peak for all 40 angles. Figure 14 presents the resolution vs. angle. Since the resolution of a peak is a measure of how spread out it is, we find that this parameter decreases (improves) near 90°.

Since these data were all for module 1 (LAD), the table below presents the resolutions for all of the modules (LAD and SPD) for 88 keV and 662 keV lines respectively at 0°.

Instrument Resolution (FWHM %)			
DM #	LAD (88 keV)	SPD (662 keV)	
	@MSFC	@MSFC	@UCSD
1	27.3	7.3	7.7
2	23.6	7.6	7.3
3	24.5	8.1	7.3
4	26.8	7.3	7.4
5	28.5	7.2	6.9
6	24.9	7.1	6.9
7	-	7.5	7.7
8	25.6	7.2	-

Finally, Figure 15 presents the measurements of peak height vs. angle. As mentioned above, the principal features are the cosine-like decrease for angles between 0° and approximately 75°, the presence of deposited energy at 90°, and the attenuated deposition at angles greater than 90°. The ability of the higher-energy gammas to penetrate through the backside of the detector is evident (compare Cs-662 keV vs. Ba-256 keV).

3. Performance Tests: TPS-59

Other tests were performed on the detectors (at normal incidence) to measure such things as detector resolution, energy vs. channel linearity, and to note any inter-detector differences. These tests carry the identification TPS-59.

As an example, Figures 16 and 17 show the differences in the recorded spectra for Large Area detectors 0, 2, and 8. In Figure 16 module 8 shows considerably more dispersion than do the other two modules. This reflects a greater lateral inhomogeneity in that detector's response to the conversion of gamma-ray energy into an electrical output. At lower energies however, (cf. Figure 17) the differences are less. This large radial response is not too disconcerting. The LAD is primarily a low-energy instrument (~100 keV). The performance of DM8 at 1275 keV is well within specifications.

Figures 18 and 19 show that the detectors are very linear in energy per channel. Although this figure presents results only for module 1, the other modules demonstrate the same linearity. For future reference, the equations for energy (in keV) as a function of channel number for modules 1, 2, and 5 for both the LAD and SPD are listed below.

$$\left.\begin{aligned} E &= 4.9504 \cdot \text{chan.\#} - 28.042 = 4.9504 \cdot (\text{chan.\#} - 5.664) \\ E &= 5.0221 \cdot \text{chan.\#} - 33.045 = 5.0221 \cdot (\text{chan.\#} - 6.580) \\ E &= 5.1374 \cdot \text{chan.\#} - 34.432 = 5.1374 \cdot (\text{chan.\#} - 6.702) \end{aligned}\right\} \quad \text{LAD}$$

$$\left.\begin{aligned} E &= 3.9931 \cdot \text{chan.\#} - 154.21 = 3.9931 \cdot (\text{chan.\#} - 38.62) \\ E &= 3.9456 \cdot \text{chan.\#} - 154.21 = 3.9456 \cdot (\text{chan.\#} - 37.45) \\ E &= 4.1855 \cdot \text{chan.\#} - 164.52 = 4.1855 \cdot (\text{chan.\#} - 39.31) \end{aligned}\right\} \quad \text{SPD}$$

The coefficients above were calculated from measurements of photopeak centroids by the GETAPEAK program (cf. Appendix B.). These centroids for module 1 are shown in Figures 18 and 19. They are derived from a gaussian fit to the right-hand side of the data peak as demonstrated in Figure 11. It is our intention to repeat these measurements and the linear regression using the centroids of the whole peak. This will certainly result in different values for the coefficients.

4. Conclusion

The measurement of gamma-ray spectra at many different angles and energies is necessary for a correct interpretation of future data from sources of unknown origin. We have discovered that one important facet of the angular response is the presence of the detector's "radial response" first mentioned in §2.3.1. This variation in crystal response as a function of distance from the center must be accurately modelled if future analyses are to be successful.

We have begun to calculate the net response of the crystal under the assumption of different response functions. We have assumed, as first approximations, that the radial response changes from 100% in the center to 85% at the edge and that this variation has a radial dependence that is 1) linear, 2) quadratic, and 3) (co)sinusoidal. The results from these calculations are in a preliminary stage and have not been included in this report. The true radial dependence could very well be a non-analytic function. Tests on the detector to be performed this fall will attempt to actually measure this function. We will then attempt to fit analytical curves to the measurements to include in future calculations.

Bibliography

1) Harding, A. K., V. Petrosian, and B. J. Teegarden, 1986, Spectra and Emission Mechanisms, Ch. 2 in *AIP Conference Proceedings*, **141**, *Gamma-Ray Bursts*, ed. by E. P. Liang, AIP, New York.

2) Price, W. J., 1964, Nuclear Radiation Detection, Second Edition, McGraw-Hill Book Company, New York.

Appendix A:

A.1 Importing the ND-76 RX-50 disks to the MSDOS format.

The Nuclear Data 76 is the instrument which records the spectra measured by the detector. It is a multichannel analyzer with an analog to digital converter (ADC). The recorded spectra can be saved on $5\frac{1}{4}$-inch disks. The format of these disks is compatible with the RX-50 standard set by the Digital Equipment Corporation.

Even though most of our data analysis will be performed on the center's mainframe computers, our microcomputers offer several advantages in their ease of use, availability of software, and speed. However, the ND-76 disks are not compatible with the MSDOS standard.

There are two methods that we considered to import the files to the PC's. The first was to try one of the many multi-format programs that allow a PC to read many different formats including CP/M, TRS-80, and Apple disks. Since the Nuclear Data disks are single-sided, quad density, this precludes the use of the 360-kbyte disk drives usually found in the IBM PC. However, the PC/AT compatibles come with 1.2 Mbyte drives. These can read the higher density. Unfortunately, none of the programs that we tested had the RX-50 format as one of its choices. This would have been the most straightforward method. We are still looking into this possibility.

The second method involved reading the ND disks directly in the RX-50 disk drive of the BATSE μVAX. Because of the DEC compatibility this was an easy task. With a disk inserted in floppy drive #1, log onto the destination directory and issue the following commands;

```
EXCHANGE
COPY $FLOPPY1:*.*  */TRANSFER=BLOCK
EXIT.
```

The files are organized in subdirectories on the VAX under the BATSE account name. The subdirectories are named DM0, DM1, ..., for the Detector Modules. Within each subdirectory there is a further set of subdirectories representing the different tests run on that module. So, for example, the spectra taken during the TPS-19 tests of module 1 are found in the directory $DISK2:[BATSE.DM1.TPS19]. VAX DCL command macros have been written to facilitate movement between these deeply-nested subdirectories. To go to the aforementioned directory, issue the DCL command: CD 1 19.

Getting the files from the VAX onto the PC's was easier than we first thought. Using an Ethernet connection the files were quickly transferred using NFT. For example, to copy all of the TPS-19 files for module 1 the commands are:

```
NFT
COPY BATSE"BATSE password"::$DISK2:[BATSE.DM1.TPS19]*.*  *
EXIT
```

Once on the PC, these files in binary format are converted into ASCII files with the CONVERT program written by the author (cf. Appendix B). The spectra were then archived on 1.2 Mbyte floppy disks.

Appendix B.

B.1 Software Development

We have written two programs for use by the BATSE team in their analysis of the test data. The first, called CONVERT, converts a spectrum from the binary format used by Nuclear Data to a straight ASCII format. These converted files can then be read into Lotus 1-2-3, or other programs. Since the MSDOS machines allow 8-character filenames (vs. 6 for the ND), we followed the following algorithm for choosing the output file name. Two examples of spectral files are LA1165.CSL and SPD1VT.NA0. The first is a (TPS-19) measurement by the Large Area detector module 1 of a cesium-137 spectrum at an angle of 165°. Since the 'L' in 'CSL' is redundant, we dropped it to form an 8-character MSDOS filename with an extension of '.prn'. In the second case, from TPS-59, the first three letters were always LAD or SPD for either the large area detector or the spectroscopy detector. We therefore dropped the 'D'. The two output files are then LA1165CS.PRN and SP1VTNA.PRN.

B.2 CONVERT.EXE

The user of CONVERT has three choices depending on the type or number of data file(s) that he is converting.

1) The simplest is one input file and therefore one output file. The user is prompted for both filenames. We recommend consistency with the above file-naming convention.

2) The second method is used for angular response files. Here there are up to 40 filenames representing the 40 angles of detector orientation. If this option is chosen, the program reads a data file (ORIENT.DAT) containing the 40, or less, angles. It also prompts the user for other pertinent information such as module number, detector, and source.

3) The final choice is used for TPS-59 data files. In this case, the root filename is constant and only the extension changes. The user is prompted for the root (e.g., LAD1VT) and the extensions are stored in a data file called 'EXTENS.DAT'.

B.3 GETAPEAK.EXE

The second program, called GETAPEAK, allows the investigator to measure the properties of spectral photopeaks. We have used it to measure centroids, resolutions, and peak heights. It also does an automatic fitting of a gaussian to the peak or portions of a peak. Further information can be gotten by running the program and pressing the F1 (HELP) key.

We plan revisions to both of these programs. The online help should be checked for any changes made after this report is filed.

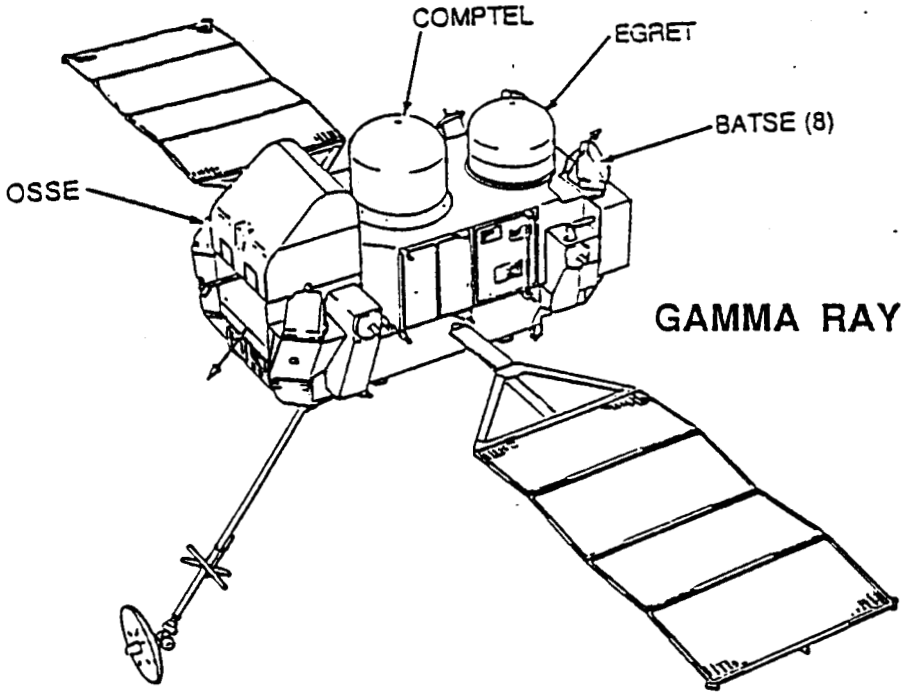

FIGURE 1

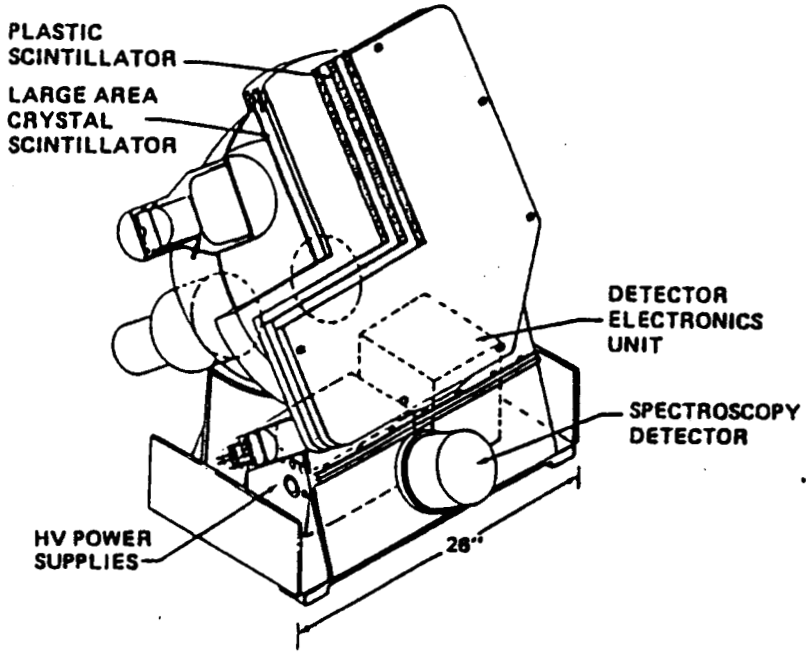

BATSE
DETECTOR MODULE
(1 OF 8)

FIGURE 2

ORIGINAL PAGE IS
OF POOR QUALITY

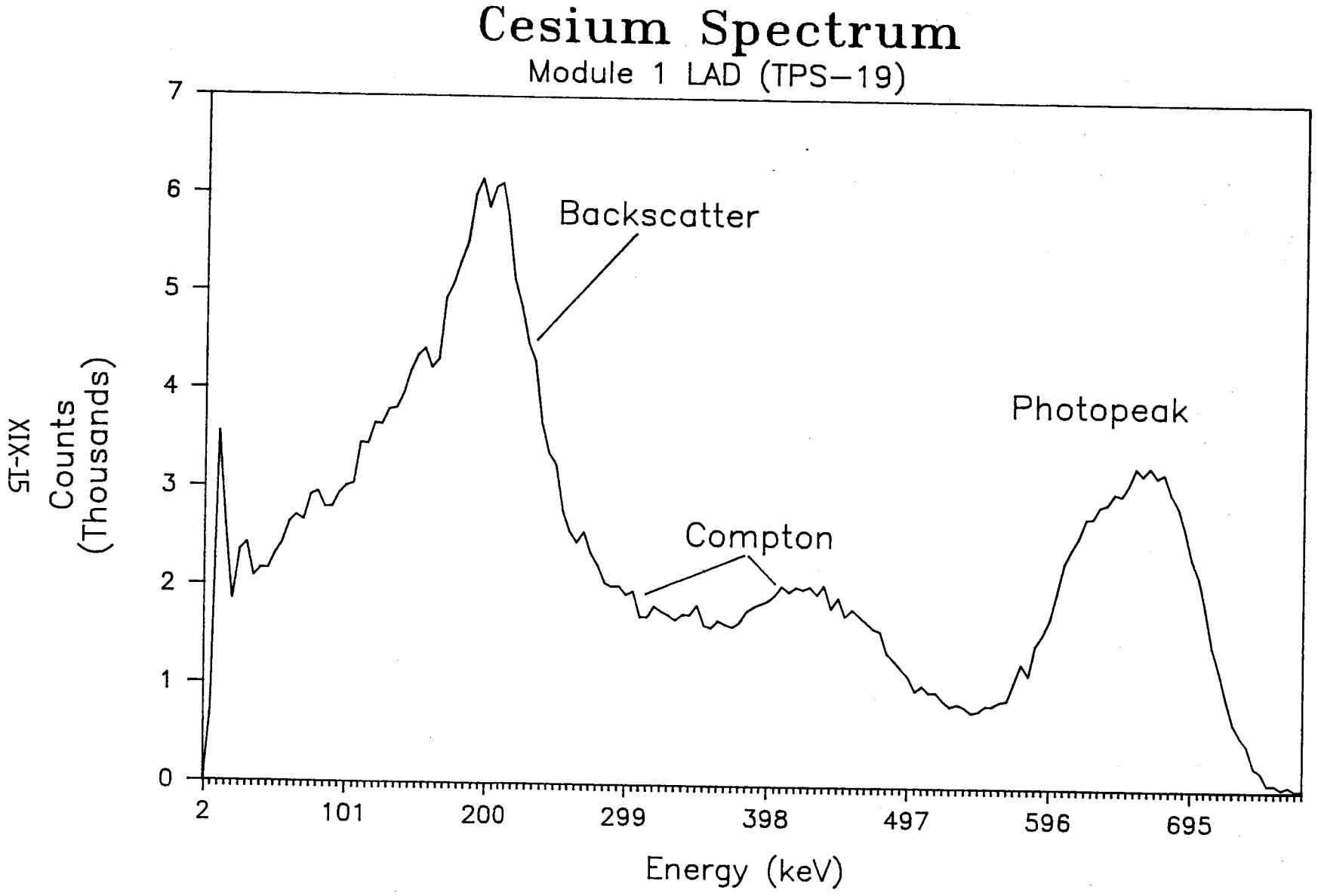
Cesium Spectrum
Module 1 LAD (TPS-19)
Counts (Thousands)
0
1
2
3
4
5
6
7
Backscatter
Compton
Photopeak
2
101
200
299
398
497
596
695
Energy (keV)

FIGURE 3

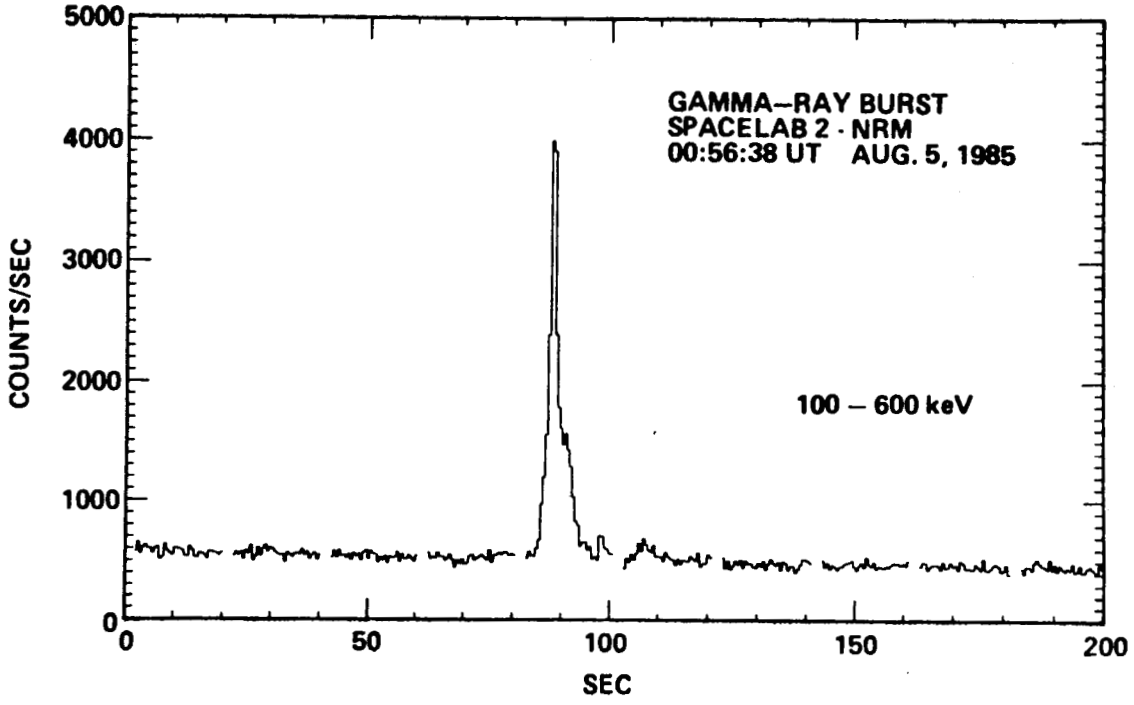

FIGURE 4

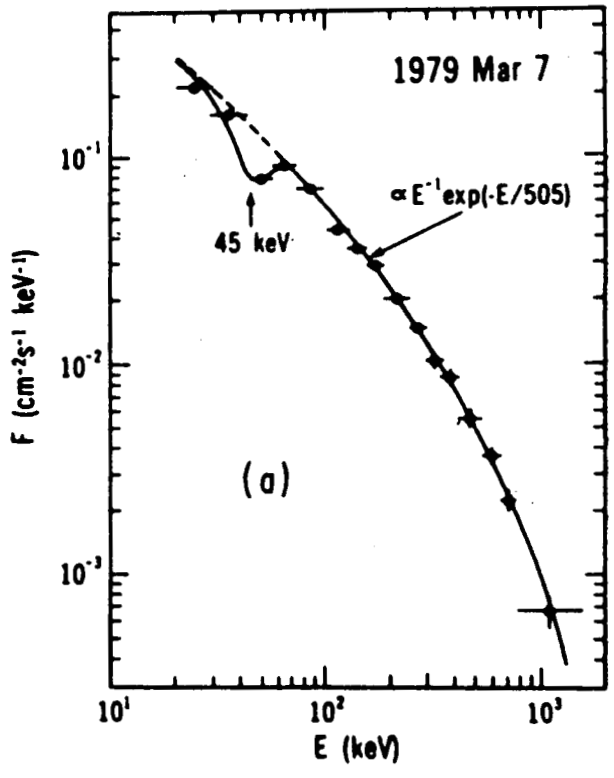

FIGURE 5

The effect of slant path on efficiency

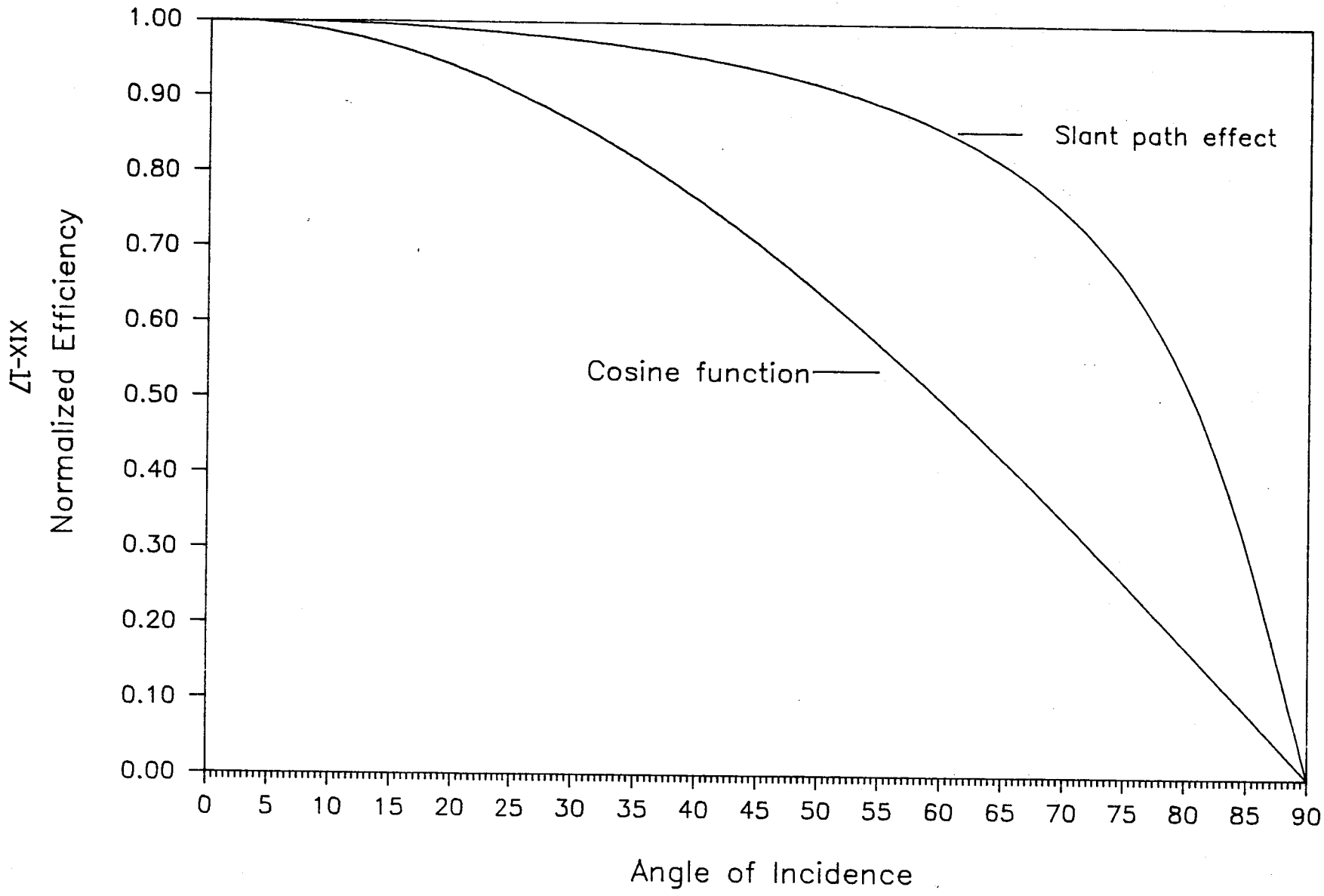

FIGURE 6

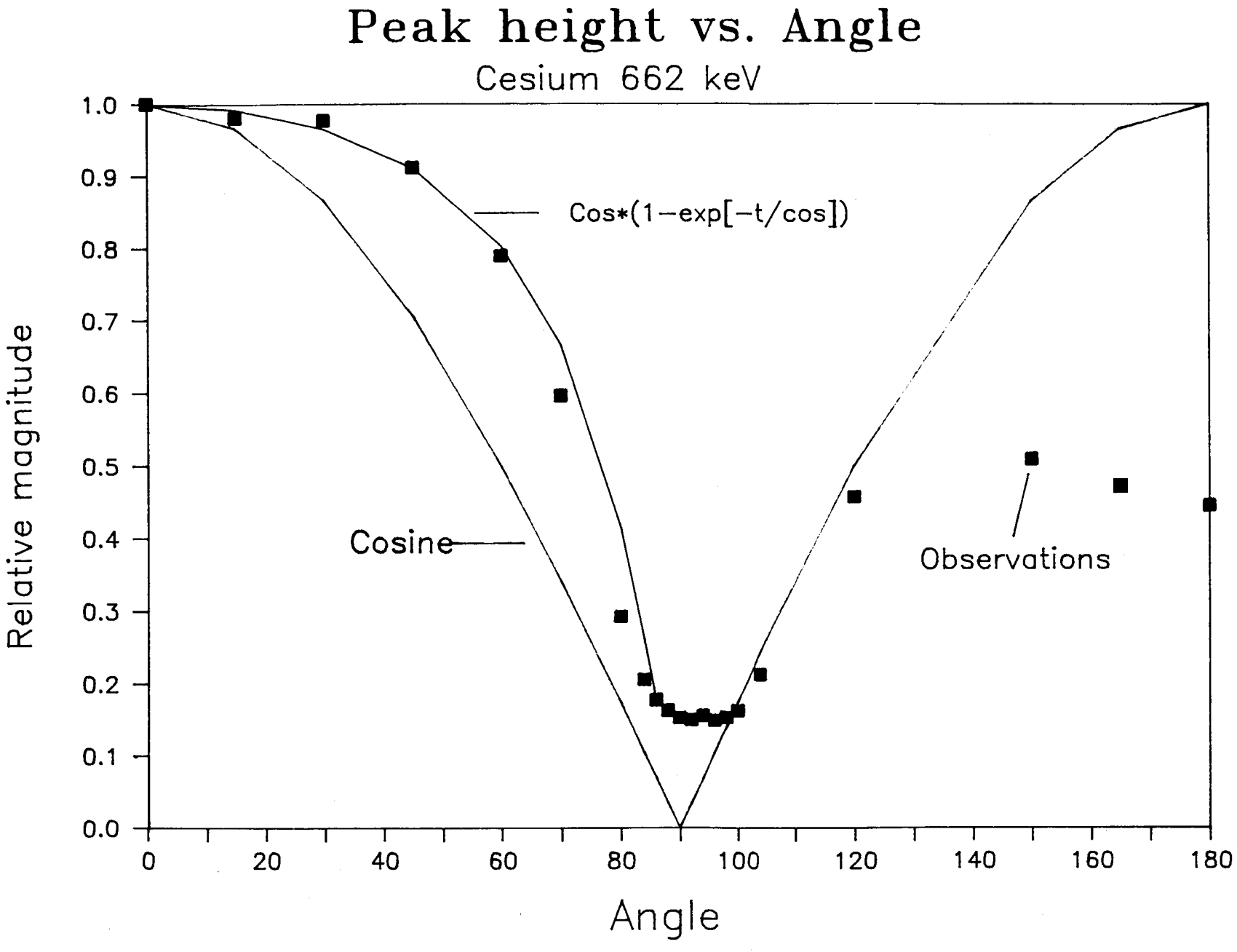
Peak height vs. Angle
Cesium 662 keV
Relative magnitude
1.0
0.9
0.8
0.7
0.6
0.5
0.4
0.3
0.2
0.1
0.0
0
20
40
60
80
100
120
140
160
180
Angle
Cos*(1−exp[−t/cos])
Cosine
Observations

FIGURE 7

Angles of Incidence
for TPS–19

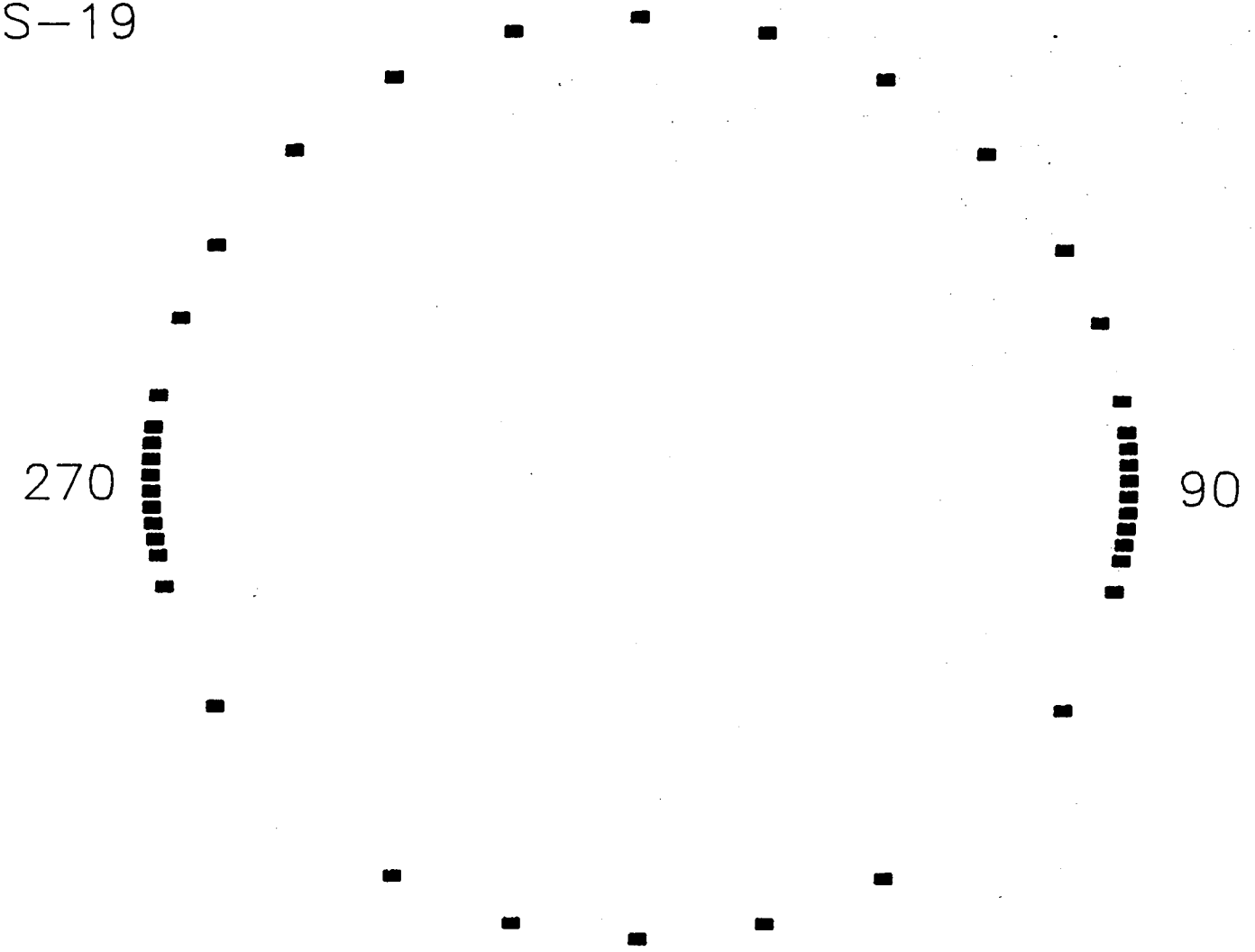

FIGURE 8

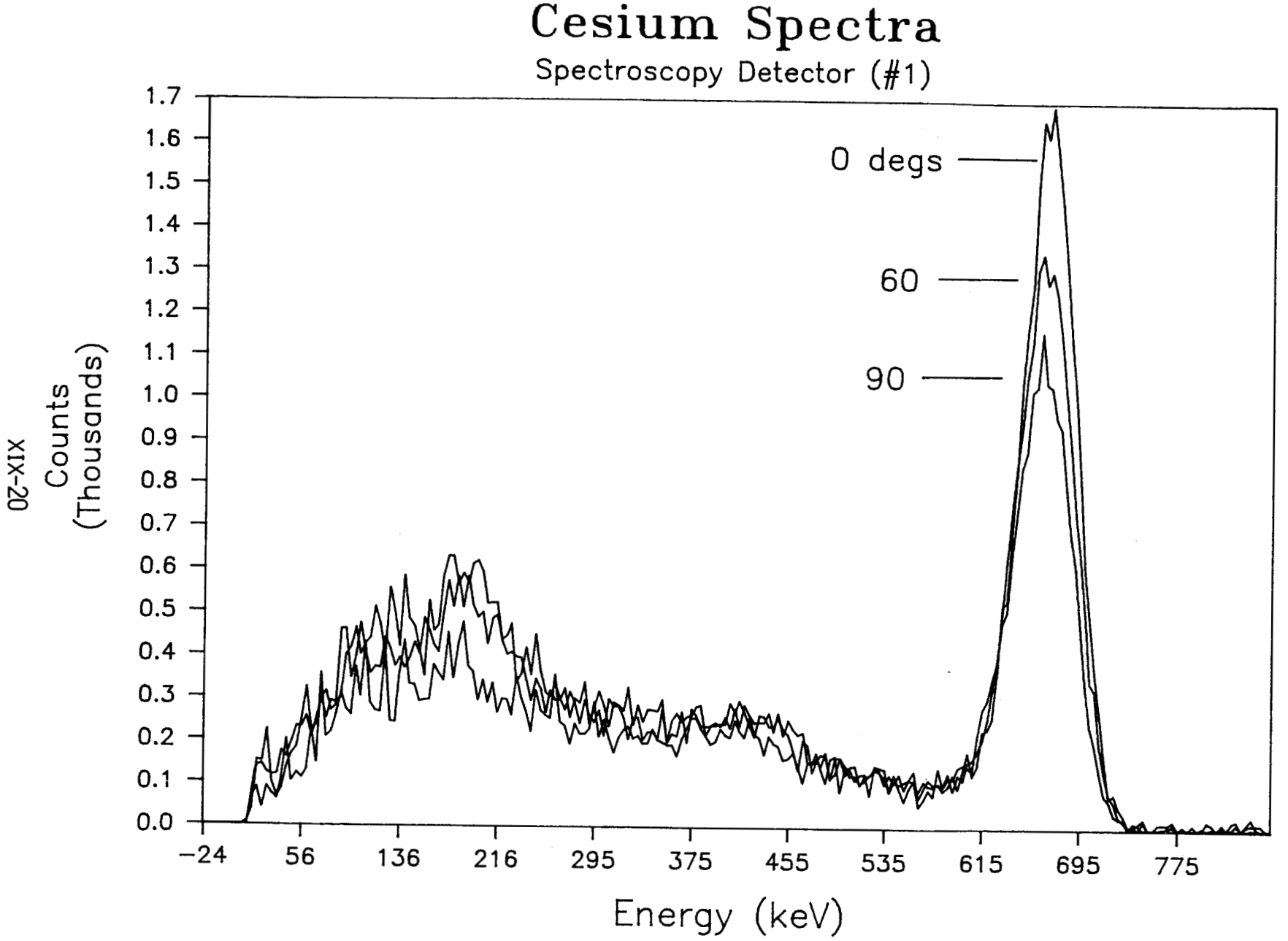
Cesium Spectra
Spectroscopy Detector (#1)
0 degs
60
90
Counts (Thousands)
1.7
1.6
1.5
1.4
1.3
1.2
1.1
1.0
0.9
0.8
0.7
0.6
0.5
0.4
0.3
0.2
0.1
0.0
-24
56
136
216
295
375
455
535
615
695
775
Energy (keV)

FIGURE 9

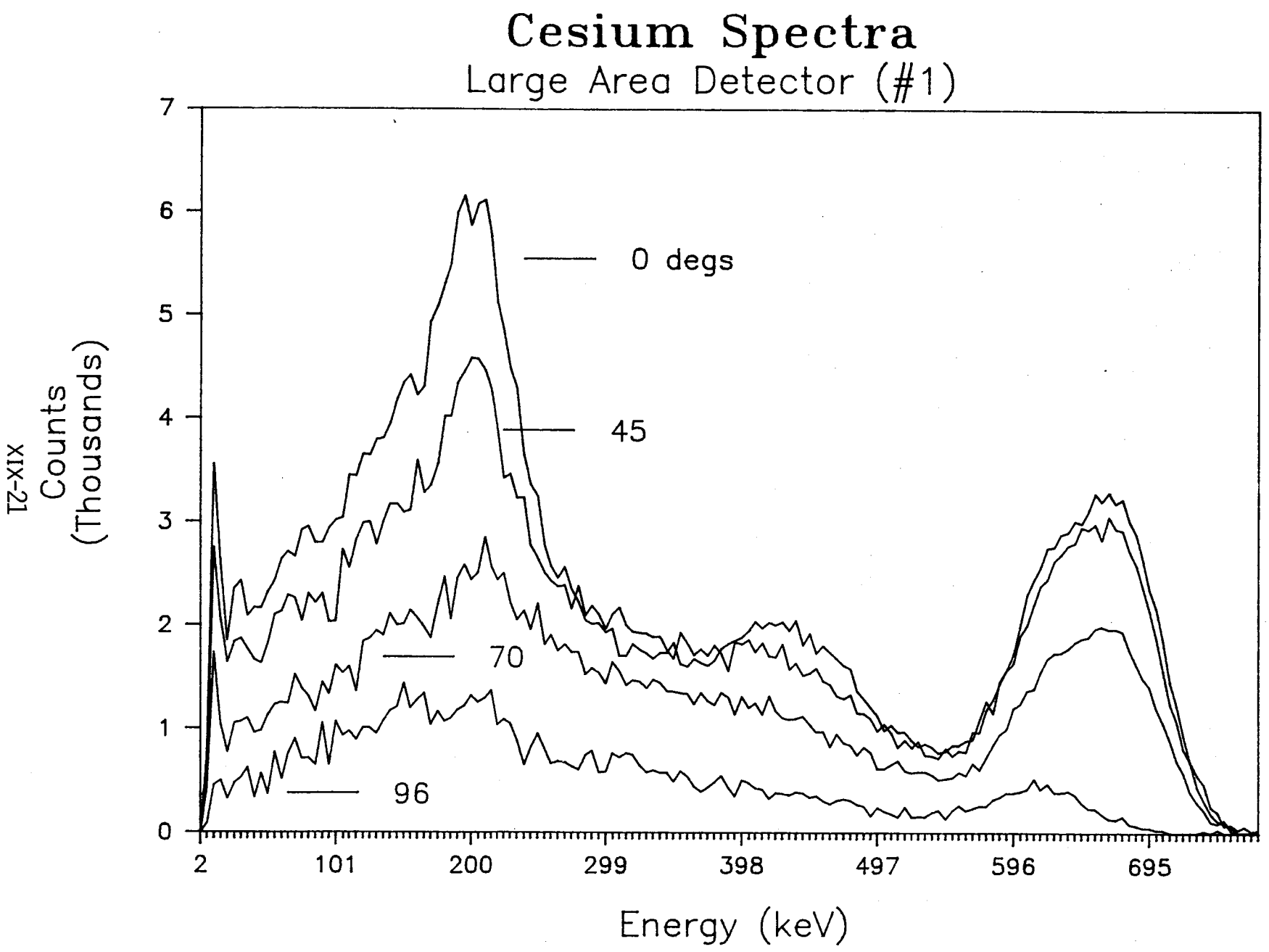
Cesium Spectra
Large Area Detector (#1)
Counts (Thousands)
7
6
5
4
3
2
1
0
0 degs
45
70
96
2
101
200
299
398
497
596
695
Energy (keV)

FIGURE 10

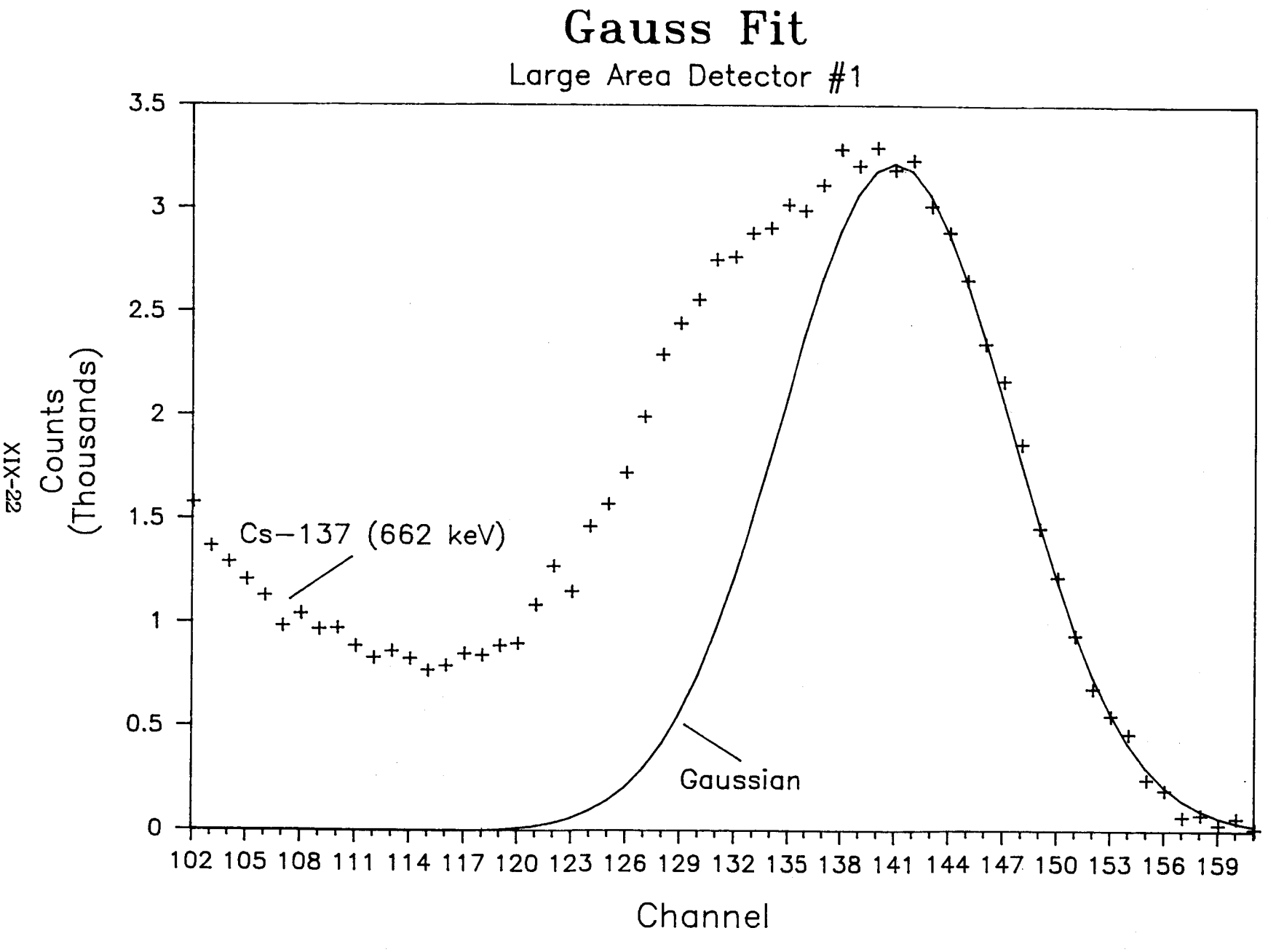
Gauss Fit
Large Area Detector #1
Counts (Thousands)
3.5
3
2.5
2
1.5
1
0.5
0
Cs−137 (662 keV)
Gaussian
102 105 108 111 114 117 120 123 126 129 132 135 138 141 144 147 150 153 156 159
Channel

FIGURE 11

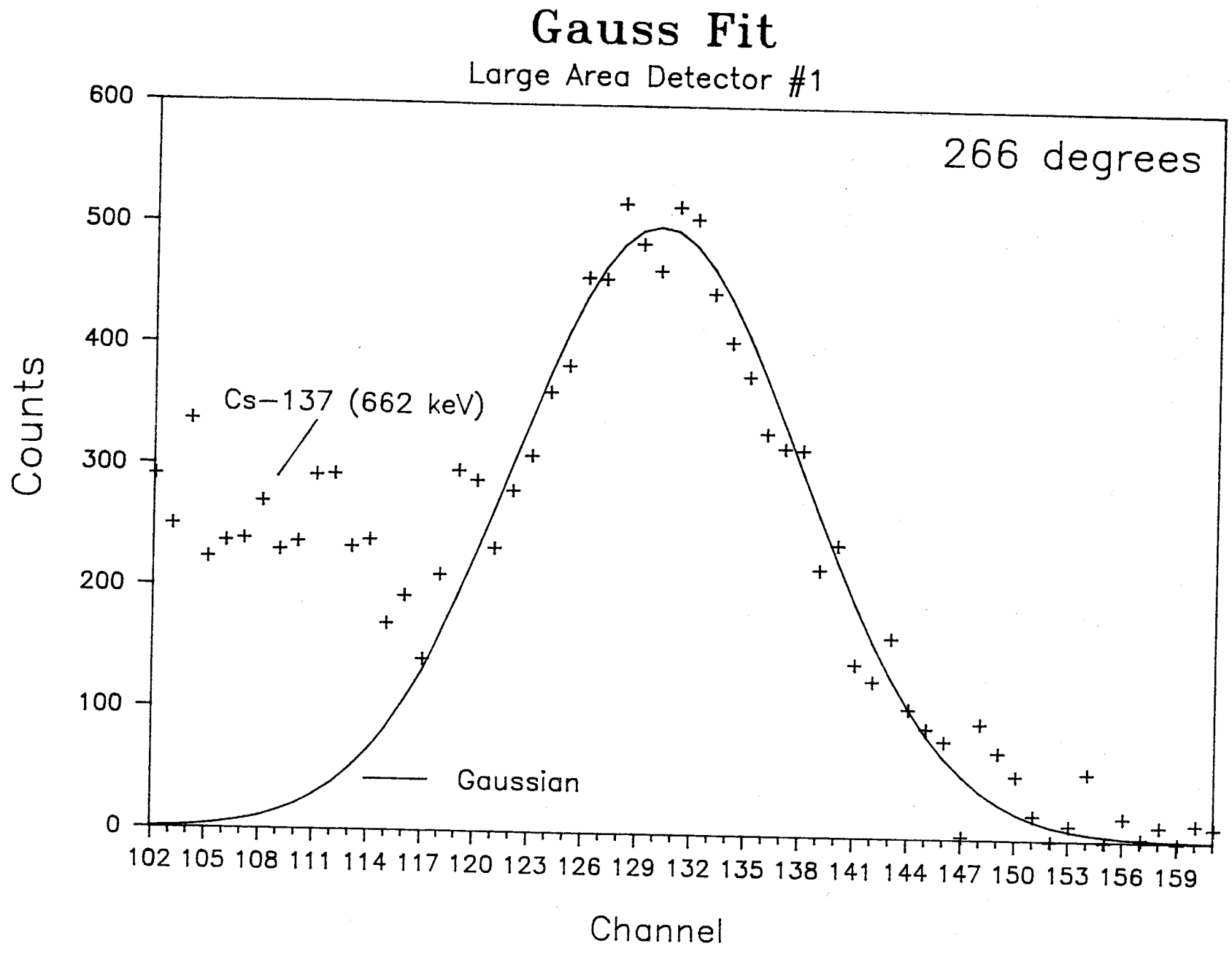
Gauss Fit
Large Area Detector #1
266 degrees
Cs-137 (662 keV)
Gaussian
Counts
Channel
600
500
400
300
200
100
0
102 105 108 111 114 117 120 123 126 129 132 135 138 141 144 147 150 153 156 159

FIGURE 12

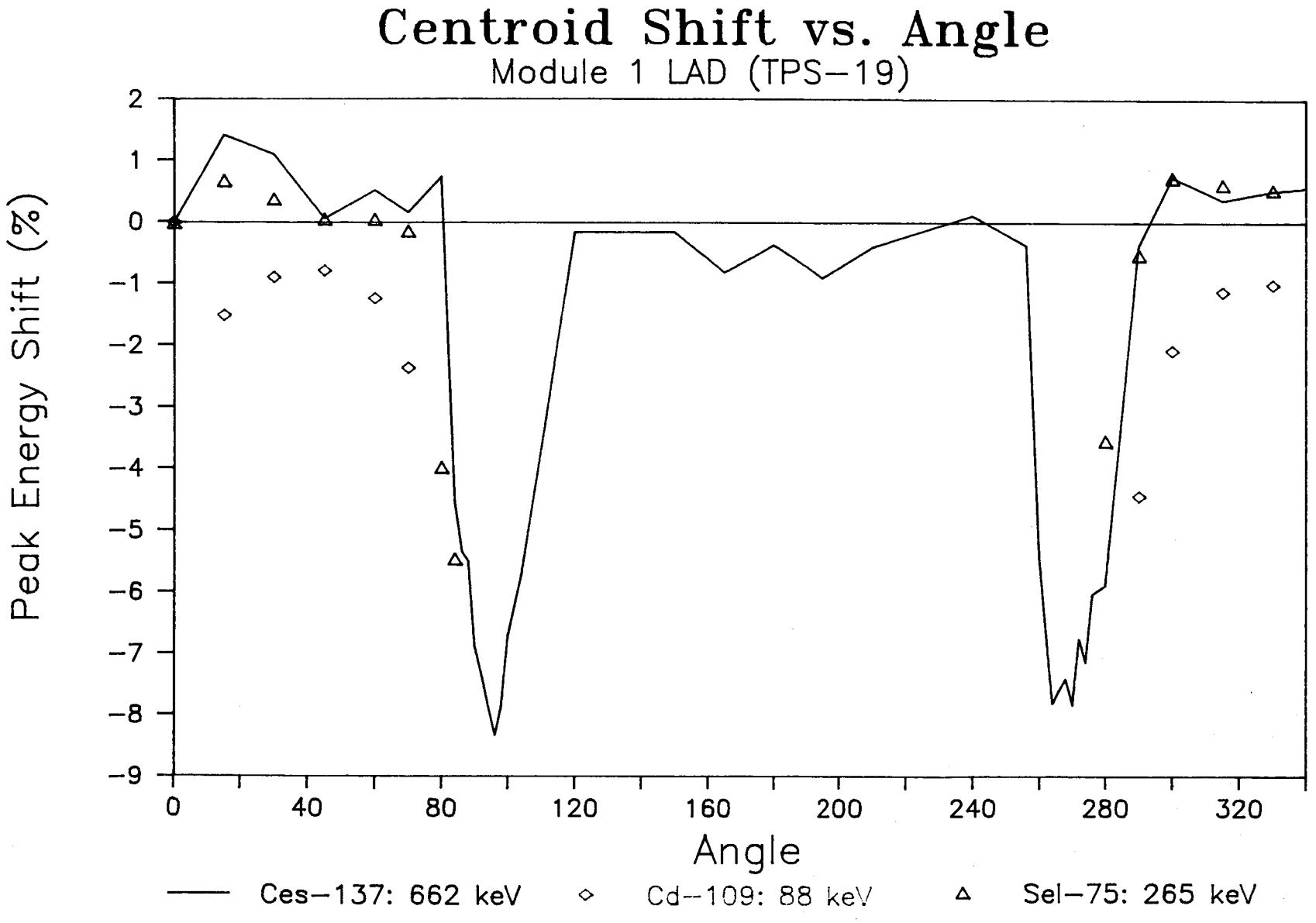
Centroid Shift vs. Angle
Module 1 LAD (TPS-19)
Peak Energy Shift (%)
2
1
0
-1
-2
-3
-4
-5
-6
-7
-8
-9
0
40
80
120
160
200
240
280
320
Angle
Ces-137: 662 keV
Cd-109: 88 keV
Sel-75: 265 keV

FIGURE 13

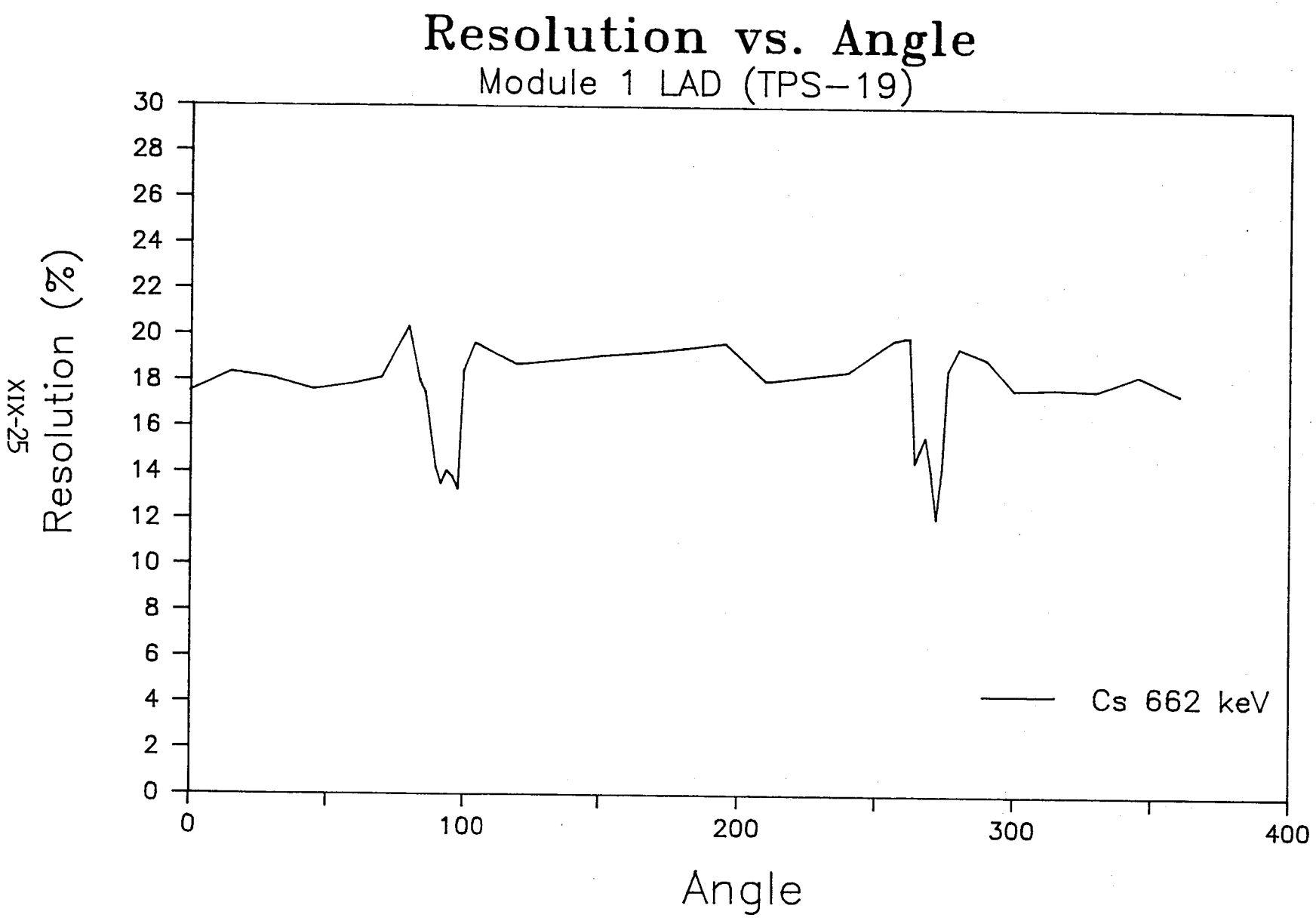
Resolution vs. Angle
Module 1 LAD (TPS-19)
Resolution (%)
30
28
26
24
22
20
18
16
14
12
10
8
6
4
2
0
0
100
200
300
400
Angle
Cs 662 keV

FIGURE 14

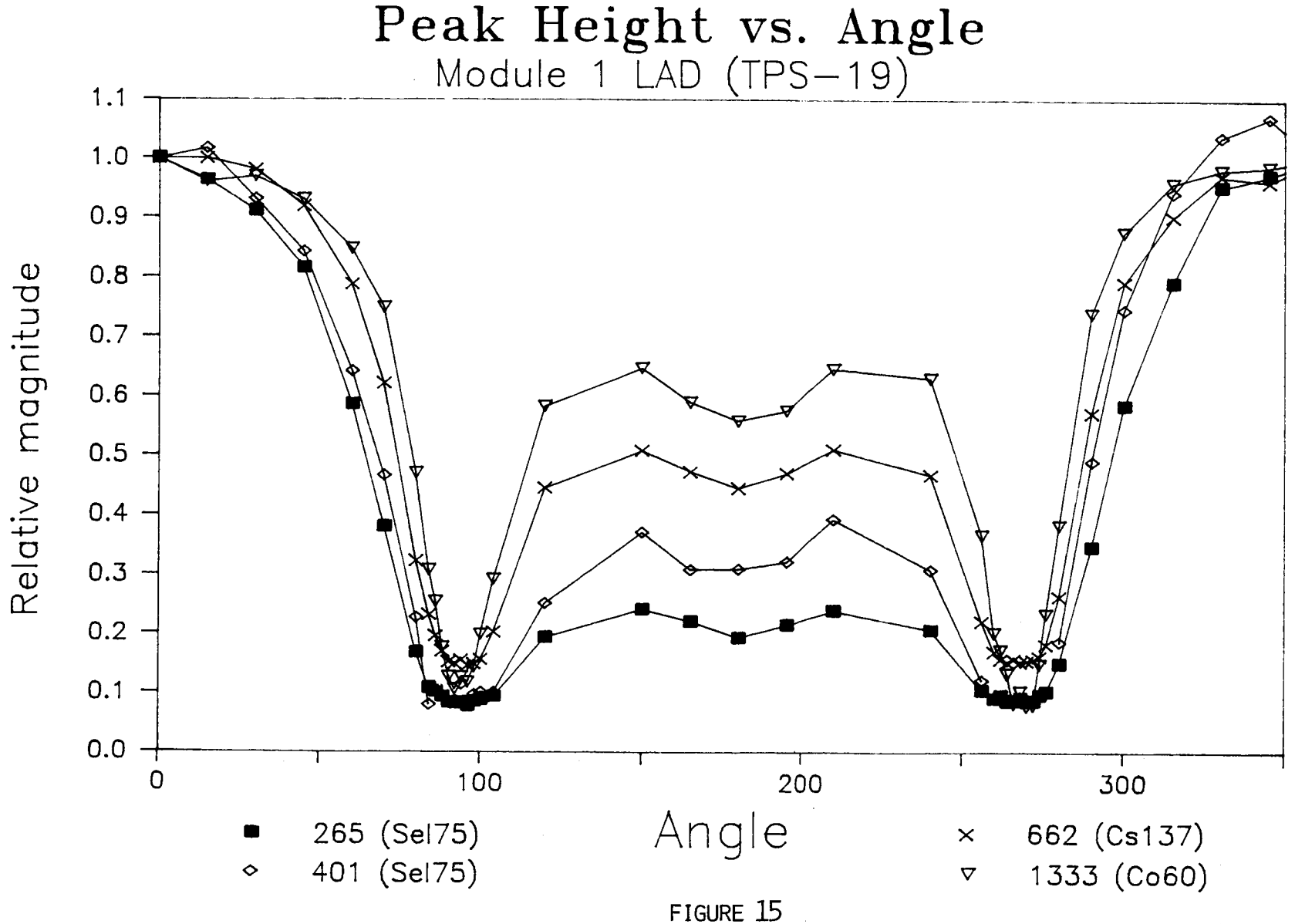
Peak Height vs. Angle
Module 1 LAD (TPS-19)
Relative magnitude
1.1
1.0
0.9
0.8
0.7
0.6
0.5
0.4
0.3
0.2
0.1
0.0
0
100
200
300
Angle
265 (Sel75)
401 (Sel75)
662 (Cs137)
1333 (Co60)

FIGURE 15

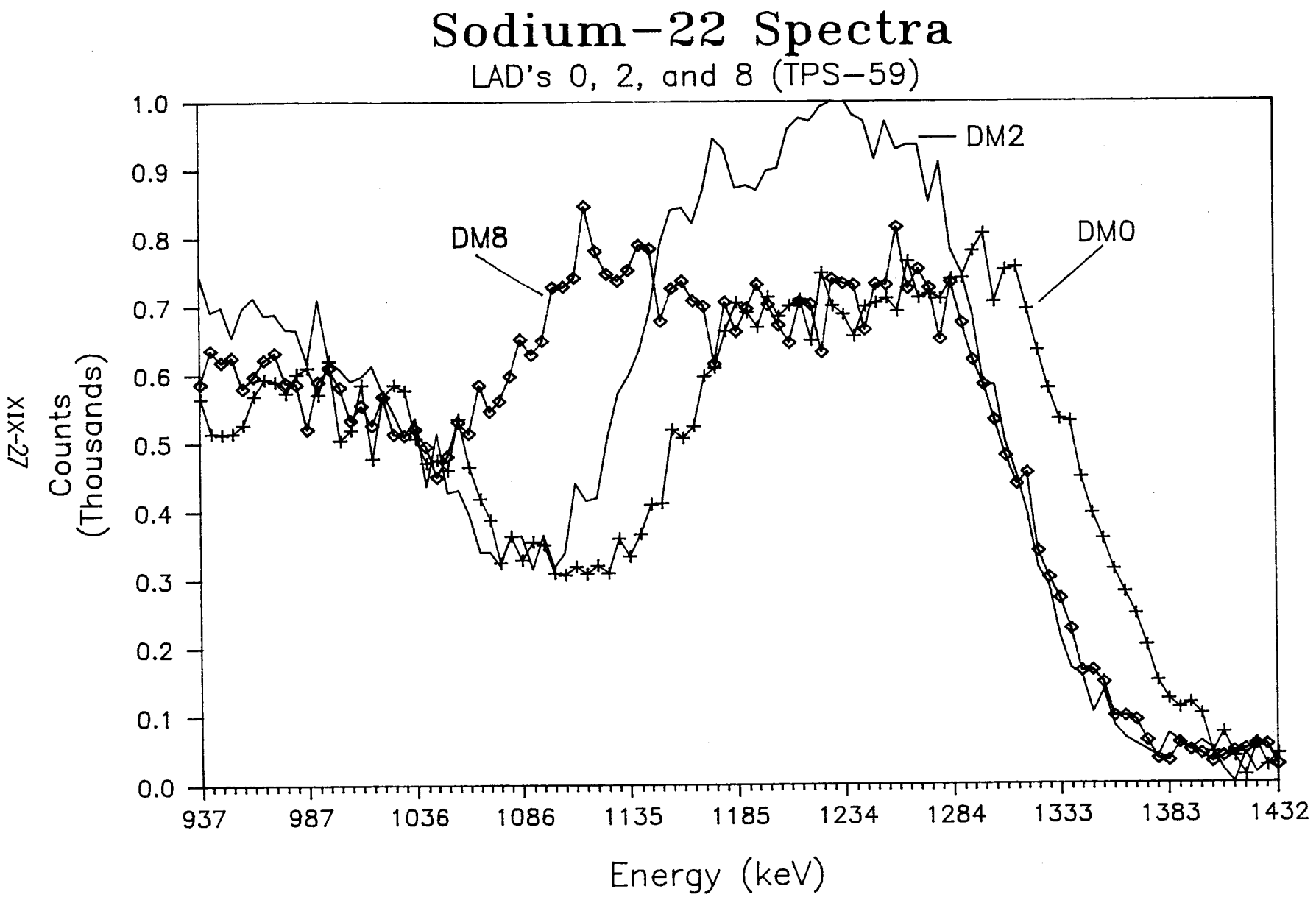
Sodium-22 Spectra
LAD's 0, 2, and 8 (TPS-59)
DM2
DM8
DM0
Counts (Thousands)
1.0
0.9
0.8
0.7
0.6
0.5
0.4
0.3
0.2
0.1
0.0
937
987
1036
1086
1135
1185
1234
1284
1333
1383
1432
Energy (keV)

FIGURE 16

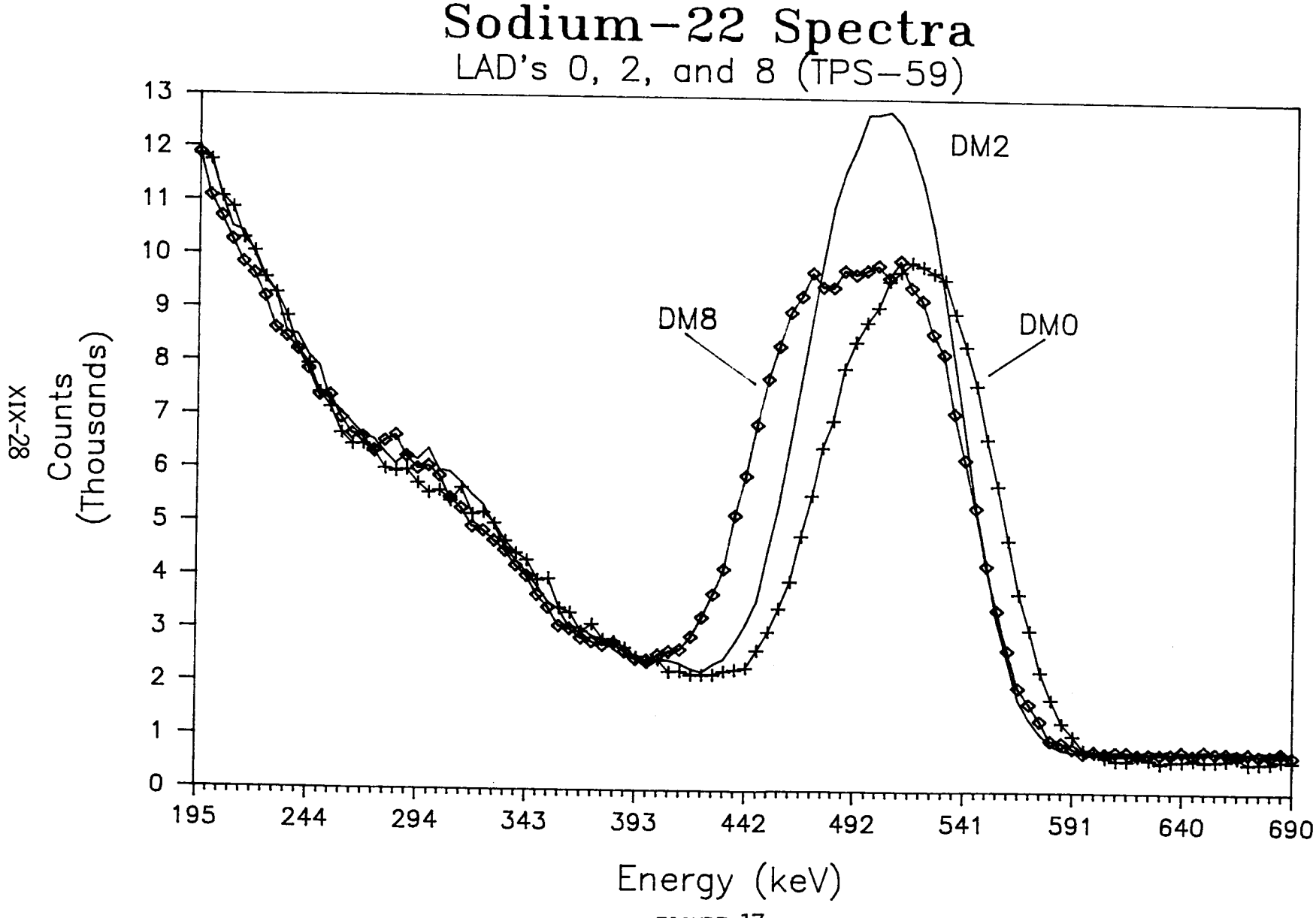
Sodium-22 Spectra
LAD's 0, 2, and 8 (TPS-59)
DM2
DM8
DM0
Counts (Thousands)
0
1
2
3
4
5
6
7
8
9
10
11
12
13
195
244
294
343
393
442
492
541
591
640
690
Energy (keV)

FIGURE 17

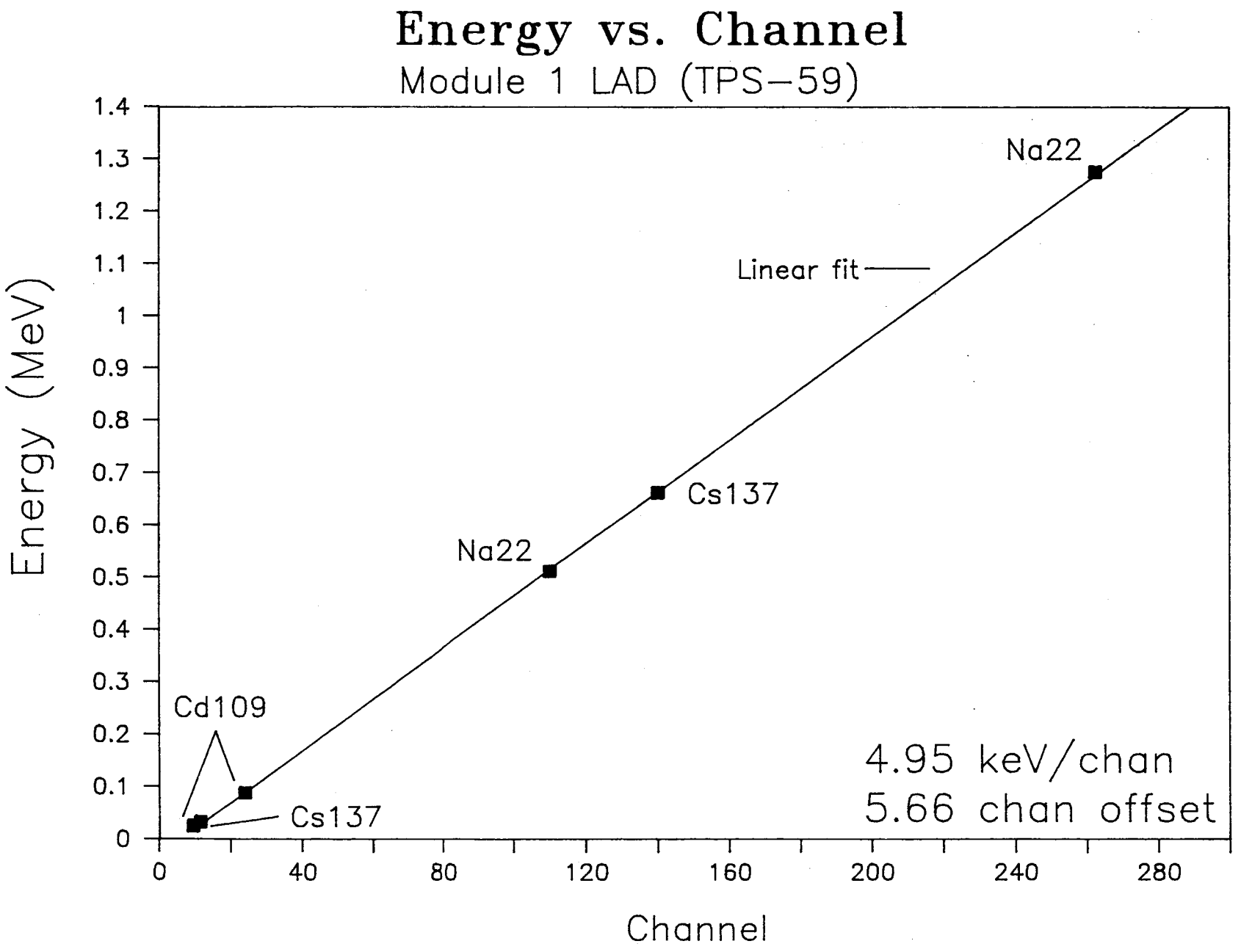
Energy vs. Channel
Module 1 LAD (TPS-59)
Energy (MeV)
1.4
1.3
1.2
1.1
1
0.9
0.8
0.7
0.6
0.5
0.4
0.3
0.2
0.1
0
0
40
80
120
160
200
240
280
Channel
Na22
Linear fit
Cs137
Na22
Cd109
Cs137
4.95 keV/chan
5.66 chan offset

FIGURE 18

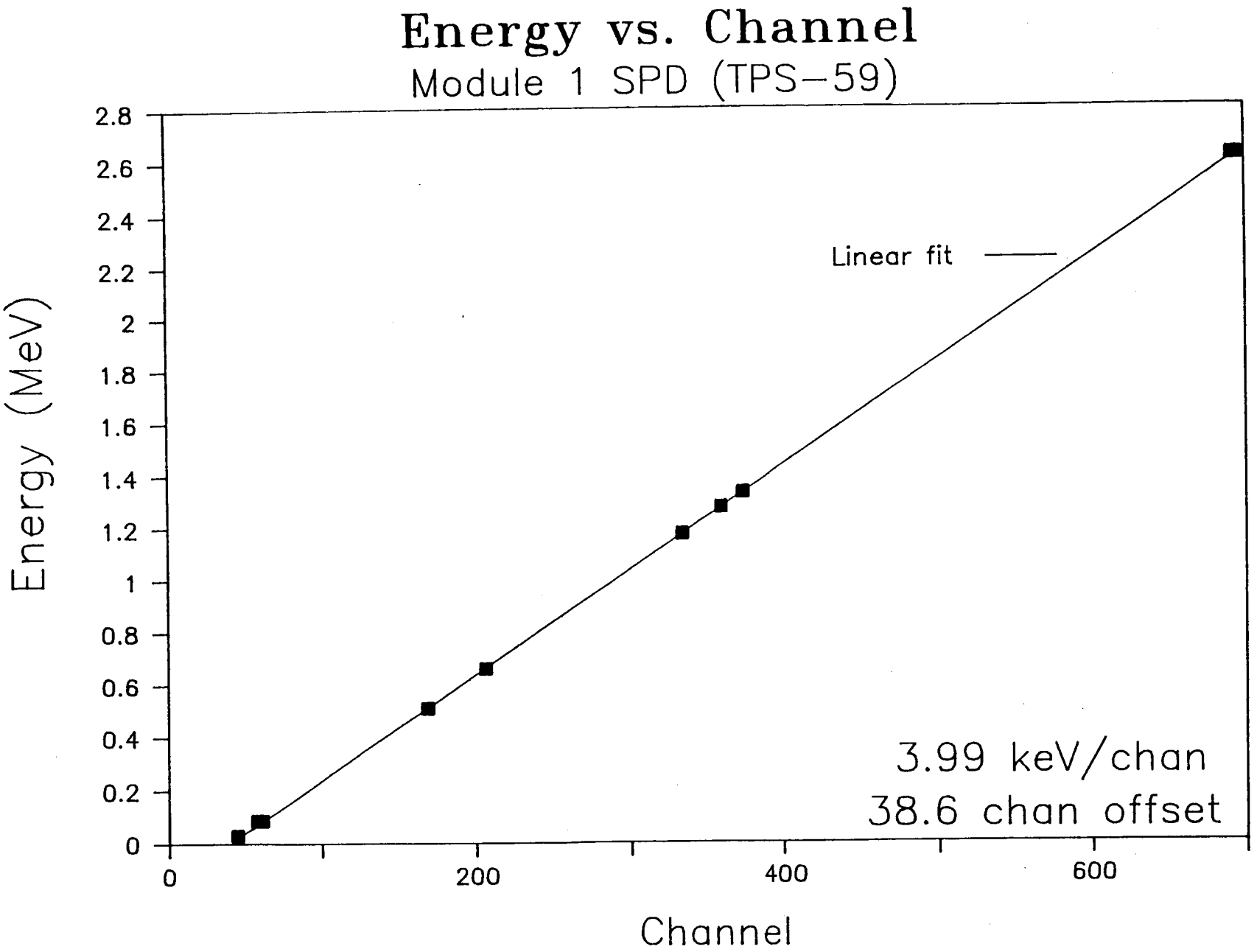
Energy vs. Channel
Module 1 SPD (TPS-59)
Energy (MeV)
2.8
2.6
2.4
2.2
2
1.8
1.6
1.4
1.2
1
0.8
0.6
0.4
0.2
0
0
200
400
600
Channel
Linear fit
3.99 keV/chan
38.6 chan offset

FIGURE 19